

# RKKY coupled local moment magnetism in $\text{NaFe}_{1-x}\text{Cu}_x\text{As}$

Yizhou Xin,<sup>1,\*</sup> Ingrid Stolt,<sup>1</sup> Yu Song,<sup>2,†</sup> Pengcheng Dai,<sup>2</sup> and W. P. Halperin<sup>1</sup>

<sup>1</sup>*Department of Physics and Astronomy, Northwestern University, Evanston IL 60208, USA*

<sup>2</sup>*Department of Physics and Astronomy and Rice Center for Quantum Materials, Rice University, Houston TX 77005, USA*  
(Dated: July 13, 2021)

A central question in a large class of strongly correlated electron systems, including heavy fermion compounds and iron pnictides, is the identification of different phases and their origins. It has been shown that the Ruderman-Kittel-Kasuya-Yosida (RKKY) interaction between localized moments, and that the competition between this interaction and Kondo effect is responsible for quantum criticality. However, conclusive experimental evidence of the RKKY interaction in pnictides is lacking. Here, using high resolution  $^{23}\text{Na}$  NMR measurements on lightly Cu-doped metallic single crystals of  $\text{NaFe}_{1-x}\text{Cu}_x\text{As}$  ( $x \approx 0.01$ ), we show direct evidence of the RKKY interaction in this pnictide system. Aided by computer simulation, we identify the  $^{23}\text{Na}$  NMR satellite resonances with the RKKY oscillations of spin polarization at Fe sites. Our NMR results indicate that magnetic order is due to both electronic itinerancy and local moments in this compound.

## INTRODUCTION

In the early days of investigation of the Kondo effect, Boyce and Slichter [1], studied magnetic interactions of a dilute magnetic Fe impurity in a non-magnetic, metallic Cu host. They observed  $^{63}\text{Cu}$  NMR satellites which they identified with atomic positions of Cu atoms in shells at varying distances from the impurity, attributed to the Ruderman-Kittel-Kasuya-Yosida (RKKY) interaction of local moments at the Fe sites, coupling through the hyperfine field to the copper nuclei. This interaction is mediated by the conduction electron spins. The satellites determine both the range and the magnitude of the RKKY oscillations in the electronic spin density. It has been shown by past studies that this interaction plays an important role in the formation of magnetic order in strongly correlated electron systems. For instance, in some heavy fermion metals, the antiferromagnetic (AFM) order is driven by the RKKY interaction among the localized  $f$ -electrons, and is proposed to compete with the Kondo effect to be responsible for quantum criticality [2–4]. For iron chalcogenides, ab initio electronic structure calculations show that this interaction stabilizes bicollinear AFM order [5].

Numerical studies of iron pnictides based on multi-band models [6] show that the RKKY interaction becomes anisotropic in  $\text{EuFe}_2\text{As}_2$  where suppression of superconductivity has been reported [7]. Magnetic suppression of superconductivity has also been attributed to RKKY-like interactions in the vicinity of Mn impurities in  $\text{LaFeAsO}_{1-x}\text{F}_x$  and  $\text{BaFe}_2\text{As}_2$  compounds [8, 9]. In these instances,  $^{75}\text{As}$  NMR spectral shifts are associated with the  $^{75}\text{As}$  nuclei that are nearest-neighbor (NN) to the Mn impurities. However, as far as we know, there is no direct experimental evidence for existence of the RKKY interaction in pnictides. It is important to explore if RKKY can be directly observed in iron pnictides taking advantage of high resolution  $^{23}\text{Na}$  NMR and then

to identify its role in the AFM state. This is what we report here.

The Cu-doped pnictide,  $\text{NaFe}_{1-x}\text{Cu}_x\text{As}$ , is distinct from other iron pnictides. In the heavily doped regime ( $x \approx 0.5$ ) it is a Mott insulator while for low copper doping concentrations ( $x \leq 0.05$ ) it is metallic, exhibiting superconductivity in close proximity to an AFM ordered state [10, 11]. At high doping long-range AFM order arises from localized moments on the Fe sites [12–16] and the Cu dopants are nonmagnetic in a valence state  $\text{Cu}^{1+}$  with completely filled  $3d$  orbitals [12, 17]. We have previously studied this regime [15, 16] using  $^{23}\text{Na}$  NMR showing that long range order is only achieved for  $x$  very close to 0.5; otherwise, the magnetic state is an spin glass as exemplified in the case  $x = 0.39$  [Fig. 1]. In contrast, for low concentrations  $x$  as we report here, the Cu dopants are found to be electron doping, suggesting that they are magnetic with valence  $2+$  [10, 18]. The magnetic Fe ions are in the same valence state as the dopants [17]. In this case, it is not yet clear whether antiferromagnetism follows a local moment picture or is itinerant, associated with Fermi surface nesting [19–26].

The magnetic Cu impurities in a metallic host makes lightly Cu-doped  $\text{NaFe}_{1-x}\text{Cu}_x\text{As}$  an ideal system for searching for RKKY interaction. Two NMR-sensitive nuclei,  $^{23}\text{Na}$  and  $^{75}\text{As}$ , are located on opposite sides of the Fe layer [Fig. 1]. Both nuclei are coupled to spin polarization of the Fe ions through transferred hyperfine interaction, providing complementary information about the magnetism in the conducting plane. However, one distinct advantage of choosing  $^{23}\text{Na}$  nucleus for NMR measurements lies in that it is associated with a significantly narrow NMR linewidth than  $^{75}\text{As}$  due to its weaker hyperfine coupling [15], allowing higher spectral resolution in probing distributions of local magnetic fields.

Using  $^{23}\text{Na}$  NMR measurements on lightly Cu-doped metallic single crystals of  $\text{NaFe}_{1-x}\text{Cu}_x\text{As}$  ( $x \approx 0.01$ ), we have discovered direct evidence for RKKY interac-

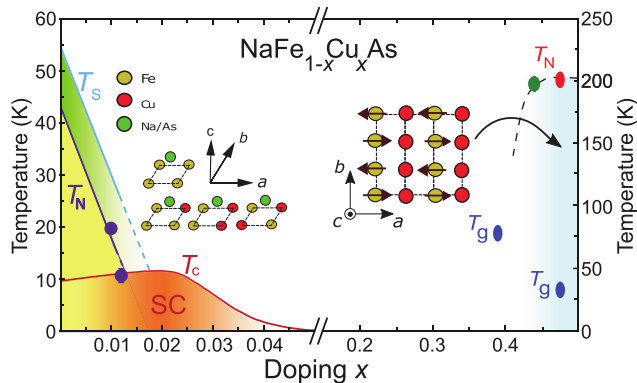


FIG. 1. Magnetic order in NaFe<sub>1-x</sub>Cu<sub>x</sub>As single crystals; phase diagram adapted from Refs [16, 29]. The system evolves from the lightly Cu-doped regime, to a correlated insulator with heavy doping. For  $x > 0.3$ , the green data point is from neutron scattering [12]; red and blue data points are from nuclear magnetic resonance (NMR) measurements [16].  $T_N$  is the Néel temperature for antiferromagnetic transitions, and  $T_g$  is the temperature of spin-glass transitions [16]. The two data points in the lightly Cu-doped regime are from this work.  $T_s$  and  $T_c$  are the temperatures of tetragonal-to-orthorhombic structural and superconducting transitions, respectively. Insets show Na and As sites relative to nearest-neighbor (NN) Fe or Cu substituted for Fe.

tion in a pnictide system for the first time. Our <sup>23</sup>Na NMR spectra of the central transition ( $1/2 \leftrightarrow -1/2$ ) reveal four satellites, which can be similarly interpreted as was the case for dilute alloys of Fe in Cu. However, there are significant differences with the Kondo system analogy. For our pnictide crystals, the pure host material exhibits antiferromagnetism with a small ordered magnetic moment,  $m \approx 0.17 \mu_B/\text{Fe}$ , and transition temperature  $T_{AF} \approx 46 \text{ K}$  [27]. Assuming a random distribution of Cu-dopants, we have simulated the corresponding hyperfine field distribution at the Na sites at room-temperature and compared with our experiment, identifying each of the <sup>23</sup>Na NMR satellites with a shell of Na nuclei. This leads to a value for the Fermi wave vector,  $k_F$ , consistent with other measurements [28], and accounts for the frequencies and spectral weight of the satellite resonances.

Furthermore, from NMR measurements of the spin-lattice relaxation rate, we find that  $1/T_1T$ , has a Curie-Weiss-like behavior above  $T_{AF}$  with a critical exponent indicative of 3D spin fluctuations in a weak itinerant AFM metal. These results are complemented by simulation of a Cu-dopant induced perturbation, and our analysis of the resulting RKKY interaction. This is very different from the non-metallic, more heavily doped, crystals of the same compound  $0.5 > x > 0.3$  [16]. Our NMR results indicate coexistence of local and itinerant magnetism in lightly Cu-doped NaFe<sub>1-x</sub>Cu<sub>x</sub>As.

## RESULTS

### Spectra

The room-temperature <sup>23</sup>Na spectra of the central transition ( $1/2 \leftrightarrow -1/2$ ) are given in Fig. 2(a) for  $x = 0.010$  and  $0.012$ . The quadrupolar satellites ( $\pm 3/2 \leftrightarrow \pm 1/2$ ) are well-resolved and an order of magnitude outside the spectral range shown here [15]. The dashed line represents the Larmor frequency,  $f_L$ , calculated from  $f_L = \gamma H_0/2\pi$ , where  $\gamma$  is the gyromagnetic ratio of <sup>23</sup>Na and  $\gamma/2\pi = 11.2625 \text{ MHz/T}$ . Both spectra show a larger component with some smaller ones. The dopant concentrations are sufficiently small that statistically they can be treated as independent impurities, Xin *et al.* [15].

In order to investigate the origin of the spectral components, we invoke a RKKY model describing a long range magnetic coupling between local moments on the Cu and Fe sites. Within this picture, the magnetic Cu<sup>2+</sup> impurities are polarized by the external field,  $\mathbf{H}_0$ , giving rise to local fields, which induce a spin polarization,  $\mathbf{s}(\mathbf{r})$ , of the conduction electrons at position specified by  $\mathbf{r}$ ;  $\mathbf{s}(\mathbf{r}) \propto \chi_{\text{RKKY}}(\mathbf{r})\mathbf{H}_0$ , with the magnetic susceptibility given by [1, 30, 31]:

$$\chi_{\text{RKKY}}(\mathbf{r}) \propto \sum_i \frac{g^2 \mu_B^2 \sin[2k_F(\mathbf{r} - \mathbf{r}_{\text{Cu},i}) + \phi]}{2k_F |\mathbf{r} - \mathbf{r}_{\text{Cu},i}|^4} - g^2 \mu_B^2 \frac{\cos[2k_F(\mathbf{r} - \mathbf{r}_{\text{Cu},i}) + \phi]}{|\mathbf{r} - \mathbf{r}_{\text{Cu},i}|^3} \quad (1)$$

where  $k_F$  is the Fermi wave vector and  $\phi$  is the average phase shift due to disorder of the dopants [32], and  $\mathbf{r}_{\text{Cu},i}$  is the location of the  $i^{\text{th}}$  Cu ion, for which the summation over  $i$  represents contributions to the susceptibility at  $\mathbf{r}$  from all Cu ions in the conduction plane. The spin-polarized conduction electrons are coupled through exchange interaction to the local moments at the Fe sites, giving rise to a transferred hyperfine field,  $\mathbf{h}_{\text{RKKY}}$ , at their near-neighbor Na nuclei,

$$\frac{\mathbf{h}_{\text{RKKY}}}{H_0} = A_{cc} \sum_{j=\text{NN}} \chi_{\text{RKKY},j}, \quad (2)$$

where  $A_{cc}$  is the transferred hyperfine field form factor given by one of the diagonal components of the the hyperfine coupling tensor (Supplementary Section I). This constant is determined by the slopes of  $K(T)$  versus  $\chi(T)$  for each <sup>23</sup>Na spectral component; inset Fig. 2(b), where  $K(T)$  is the frequency shift determined by  $K(T) = \Delta f/f_L = (f(T) - f_L)/f_L$ , and  $\chi(T)$  is the bulk susceptibility. Thus the hyperfine field at any Na site is a sum of the hyperfine coupling to its nearest-neighbor (NN) Fe atoms, at  $\mathbf{r}_j$  ( $j = 1-4$ ). To verify this RKKY model, we performed a computer-simulation of the room-temperature <sup>23</sup>Na spectrum shown for  $x = 0.012$ ; the

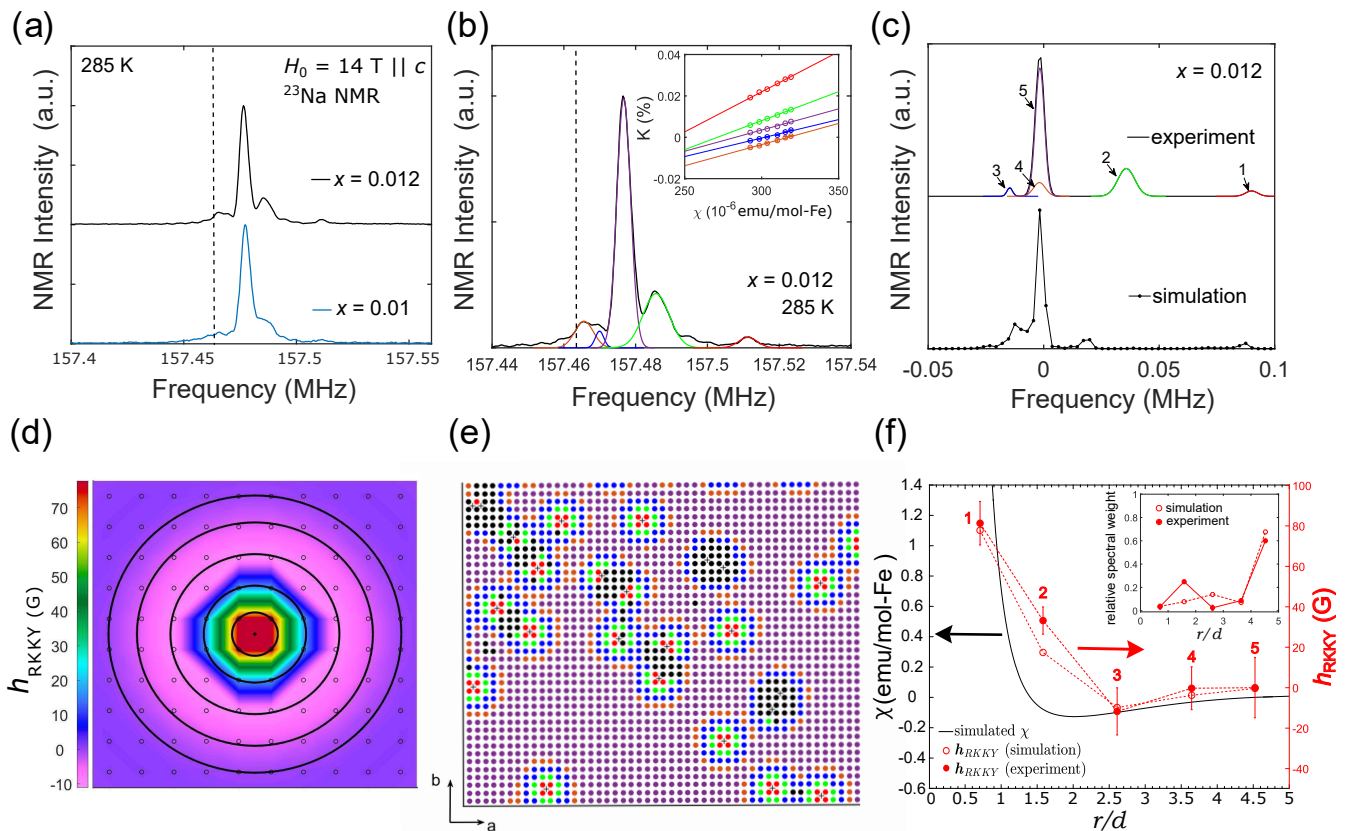


FIG. 2. RKKY interactions for  $x \approx 0.01$  (a) Room-temperature  $^{23}\text{Na}$  spectra of  $\text{NaFe}_{1-x}\text{Cu}_x\text{As}$  for the central transition ( $-1/2 \leftrightarrow 1/2$ ),  $H_0 = 14 \text{ T} \parallel c$ -axis for  $x = 0.010$  and  $0.012$ . (b) For  $x = 0.012$ , gaussian fits of spectral components indicated by color. The inset,  $K(T)$ , versus bulk susceptibility,  $\chi(T)$ ,  $125 \text{ K} \leq T \leq 250 \text{ K}$  for each spectral component; the slopes are the hyperfine fields. (c) Comparison of the RKKY model with experiment, corrected for the orbital shift,  $K_o$  obtained from b). (d) Calculated hyperfine fields in the  $ab$ -plane,  $h_{\text{RKKY}}$ . Na sites are small black open circles near the Cu dopant (black cross). Large black circles label shells of Na sites color coded in b), c) and e). (e) Larger view of the simulation field. (f) Black trace is the susceptibility  $\chi_{\text{RKKY}}$  versus radial distance  $r/d$  from a Cu dopant. The data points are measurements of hyperfine fields for Na in different shells. The numbers correspond to the different spectral components in c). The inset shows a comparison of relative spectral weights between the simulated and experimental results for each spectral component.

simulated spectrum is essentially a histogram of the hyperfine fields at the Na sites.

However, Eq. 2 only addresses the magnetic coupling in the spin degrees of freedom. The frequency shift measured for each  $^{23}\text{Na}$  spectral component, shown in Fig. 2(b) must be corrected for the temperature independent orbital contribution,  $K_o$ , given by linear extrapolation of  $K(\chi)$  to zero (inset Fig. 2(b)), for each spectral component. The orbital-corrected spectrum, can then be compared with the simulation shown in Fig. 2(c). The simulation was performed with a  $800 \times 800$  Fe lattice, randomly populated by Cu dopants with a probability  $p = 0.012$ . A small portion of the simulated Fe-Cu lattice is depicted in Fig. 2(e), showing a broader view of  $h_{\text{RKKY}}$  at each Na site. Five concentric shells of Na sites, centered at a single Cu dopant are identified [Fig. 2(d)], associated with the spectral components labeled from smallest to largest in Fig. 2(c). Each shell represents

a group of Na nuclei contributing to one of the spectral components. The radius of each shell is determined by the average distance of the corresponding Na sites to the Cu-dopant in the  $ab$ -plane, with the exception of the 5<sup>th</sup> shell which corresponds to all Na sites contributing to the main spectral component. The dependence of the simulated  $\chi_{\text{RKKY}}$  on distance,  $r$ , from a single impurity at the origin, is shown in Fig. 2(f), revealing a damped oscillation between ferromagnetic and antiferromagnetic coupling. At short distance ( $r \lesssim d$ ), the RKKY interaction is ferromagnetic. In the same figure, we compare the average  $h_{\text{RKKY}}$  associated with each spectral component between the simulated and orbitally corrected experimental spectra. The reasonable agreement is within experimental uncertainty. We also compare the relative spectral weight associated with each spectral component between the two, as shown in the inset of Fig. 2(f). This comparison shows a good agreement with the exception of the

spectral component color coded green in Fig. 2 (b) and (c). We note the possible existence of additional Na sites contributing to this particular spectral component, which are not considered in our model. Indeed, our assumption of RKKY interaction in the form of Eq. 1 could break down in small regions of the lattice where more than one dopants are located relatively close to one another. Incidentally, these regions are occupied by Na sites that are colored black in Fig. 2(e), contributing to none of the spectral components based on our model. Overall, our model provides a good representation of the field distribution at Na nuclei due to the RKKY interaction among the local moments at the Fe and Cu sites. Direct hyperfine coupling between Na and conduction electrons is neglected.

For the fit of the NMR spectrum to the RKKY model, we chose  $k_F \approx 0.18\pi/d$ , where  $d$  is the lattice spacing between two NN Fe atoms. This value is reasonable for iron pnictides with a Fermi surface composed of both hole and electron pockets [28]. The average phase shift owing to the random distribution of the dopants was found to be  $\phi \approx 0.8\pi$ .

In addition to the RKKY model, one might attribute the  $^{23}\text{Na}$  NMR satellites to inequivalent Na sites, each of which is associated with a different number of nearest-neighbor Fe sites occupied by a Cu dopant, similar to that discussed in Ref. [15] for the more insulating compounds  $x > 0.1$ . However, if this were the case, the scarcity of these sites due to low Cu concentration would lead to satellites of spectral weight that is at least an order of magnitude smaller than what has been observed from the NMR spectra which we report here.

### Spin-Lattice Relaxation

Spin-lattice relaxation measurements can be very informative regarding the nature of AFM order in pnictide compounds as demonstrated by Ning *et al.* [22], Dioguardi *et al.* [33, 34], and Oh [35] in their  $^{75}\text{As}$  studies of the Ba122 system and with  $^{23}\text{Na}$  NMR in Co doped Na111 compounds by Oh *et al.* [36]. Our data for  $1/T_1T$  of the main spectral component in both  $x = 0.010$  and  $0.012$ , for  $H_0 \parallel c$ -axis, is presented in Fig. 3(a). These measurements probe spin dynamics at nonzero wave vector  $\mathbf{q}$  and are related to the imaginary part of the  $\mathbf{q}$ -dependent dynamic susceptibility  $\chi''$ :  $1/T_1T \sim \sum_{\mathbf{q}} |A(\mathbf{q})|^2 \chi''(\mathbf{q}, f_L)/f_L$ , where  $A(\mathbf{q})$  is the form factor of the hyperfine interaction between the electronic and nuclear spins. The  $1/T_1T$  versus  $T$  data were fit to a combination of pseudogap and Curie-Weiss-like terms,  $1/T_1T = (1/T_1T)_{\text{pg}} + (1/T_1T)_{\text{AF}} = [A \exp(-\Delta_{\text{pg}}/k_B T) + B] + C/(T - T_{\text{AF}})^\gamma$ , where the critical exponent is  $\gamma = 0.5$  [22, 33, 37]. The effects of the pseudogap on  $K(T)$  and  $1/T_1T$ , over a range of com-

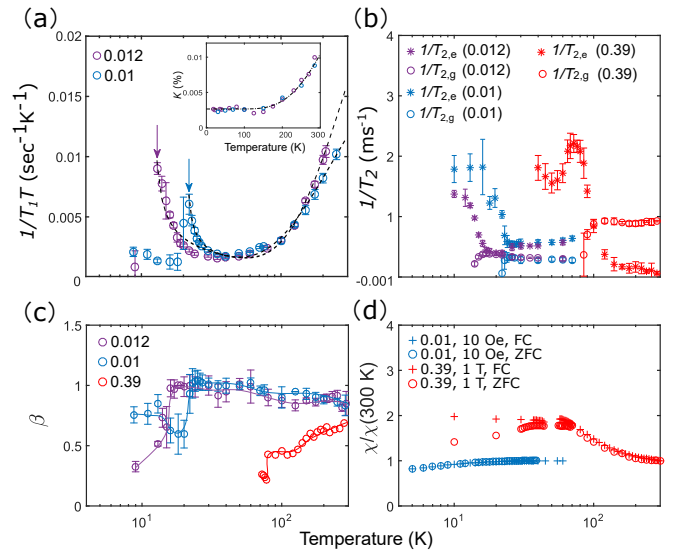


FIG. 3. Magnetic transitions. (a) Spin-lattice relaxation ( $1/T_1T$ ) measurement measured for the central transition of the main spectral component in  $x = 0.012$  and  $0.01$ . The dashed and solid lines are fits that capture both a pseudogap and a Curie-Weiss-like behavior of the data. The fits give  $T_{\text{AF}} \approx 11$  K and  $20$  K for  $x = 0.012$  and  $0.01$  respectively, marked by arrows. At high temperatures both  $K(T)$  (inset) and  $1/T_1T$  are due to the pseudogap. (b) Gaussian and exponential components of the spin-spin relaxation rate ( $1/T_2$ ). (c) Stretched exponent  $\beta$ . (d) Bulk magnetic susceptibility for  $x = 0.010$  and  $0.39$ , with  $H = 10$  Oe and  $1$  T  $\parallel ab$ . The bifurcation between data field-cooled (FC) and zero-field-cooled (ZFC) conditions for  $x = 0.39$  demonstrates a classic manifestation of spin-glass, absent for  $x \approx 0.01$ .

position, die out at low temperatures as previously reported [15, 16]. At temperatures,  $T \lesssim 40$  K,  $(1/T_1T)_{\text{AF}}$  becomes dominant and the critical exponent of  $\gamma = 0.5$  corresponds to 3D spin fluctuations due to weak itinerant antiferromagnetism [37] at the AFM wave vector  $\mathbf{q}_{\text{AF}} = (\pi/d, 0)$  [38]. This interpretation is consistent with the observed temperature independent behavior of  $\chi(\mathbf{q} = 0)$  probed by  $K(T)$  in the same temperature range, inset Fig.3(a). In contrast, the critical exponent clearly deviates from  $0.5$  for compounds in the heavily-doped regime. Setting  $\gamma$  as a free parameter for fitting, we obtain for comparison,  $\gamma \approx 1.5 \pm 0.1$  and  $1.57 \pm 1.30$  for  $x = 0.39$  and  $0.48$ , respectively (Supplementary Section III). We infer that the magnetic state evolves from itinerant to localized as  $x$  exceeds  $\sim 0.3$  [39].

Despite these differences, we note that the magnetic transition in  $x = 0.010$  and  $0.012$  share some similarity with that in  $x \gtrsim 0.3$ : (i) the magnetization recovery from the spin-lattice relaxation exhibits a stretched exponential behavior (Supplementary Section II) with  $T$  approaching the AFM transition temperature  $T_{\text{AF}}$  [Fig. 3(c)], indicating a distribution of relaxation rates, (ii) the fraction of  $^{23}\text{Na}$  nuclei contributing to the NMR spectrum,  $N_0$ , diminishes with decreas-

ing temperature, and (iii) the spin-spin relaxation rate  $1/T_2$  can be separated into gaussian  $T_{2,g}$  and the exponential  $T_{2,e}$  components (Supplementary Section II). A crossover from the former to the latter occurs as the temperature approaches  $T_{AF}$  [Fig. 3 (b)]. These observations are strong indications of inhomogeneous local magnetic fields, and is a general signature of glassy magnetic phases at low temperatures [34, 40]. This is also the case for large  $x = 0.39$  [16]. However, it is unlikely that the inhomogeneity of local fields for  $x = 0.010$  and  $0.012$  is due to magnetic frustration in contrast with  $x = 0.39$ . We note that a majority of the Na nuclei that contribute to the main spectral component are sufficiently far from Cu dopants that near neighbor Fe atoms cannot be frustrated due to competing RKKY interactions. Furthermore, the independence of Cu dopants in  $x = 0.010$  and  $0.012$  precludes significant structural disorder leading to magnetic frustration as is the case for  $x = 0.39$  [16]. This inference is also consistent with the fact that the stretched exponent  $\beta$  for  $x = 0.010$  and  $0.012$  only starts to decrease from  $\beta = 1$  close to  $T_{AF}$ , Fig. 3 (c). In contrast,  $\beta$  for  $x = 0.39$  is clearly already suppressed at room temperature, indicating intrinsic magnetic inhomogeneity and frustration due to the aforementioned structural disorder caused by dopants. The time recovery of both the spin-lattice and spin-spin relaxation is discussed in Supplementary Section II. No obvious bifurcation has been observed between the bulk susceptibility  $\chi(T)$  taken under zero-field-cooled (ZFC) and field-cooled (FC) conditions for  $x = 0.010$ , even for the small applied field  $H = 10$  Oe, as shown in Fig. 3 (d). This offers further evidence of negligible frustration effects in  $x = 0.010$  and  $0.012$ .

The  $^{23}\text{Na}$  linewidth associated with all spectral components increases substantially by at least a factor of  $\sim 3$  at low temperatures, rendering the satellites difficult to be resolved. To determine the origin of the magnetic inhomogeneity in  $x = 0.010$  and  $0.012$ , we compared our spectra for the central transitions with a simulation for the distribution of local fields. We adopted a gaussian model to describe the AFM background in which the magnetic moments at Fe sites point along the crystalline  $a$ -axis and are suppressed in the vicinity of Cu dopants [33],

$$\begin{aligned} \chi_{AF}(\mathbf{r}_{Fe}) &= C_0 \cos(\mathbf{q}_{AF} \cdot \mathbf{r}_{Fe}) \\ &\times \left\{ 1 - C_1 \sum_i \exp[-|\mathbf{r}_{Fe} - \mathbf{r}_{Cu,i}|^2/2\xi^2] \right\} \\ &= C_0 (-1)^{n_a} \left[ 1 - C_1 \sum_i \exp(-|\mathbf{r}_{Fe} - \mathbf{r}_{Cu,i}|^2/2\xi^2) \right] \end{aligned} \quad (3)$$

where  $\mathbf{q}_{AF} = (\pi/d, 0)$  [38], and  $\xi$  the length scale of this suppression. The constant  $C_0$  represents the magnitude of the AFM ordered moment and  $C_1$  the suppression. Thus the total hyperfine field  $h_{\text{total}}$  at a Na nucleus be-

comes,

$$\begin{aligned} \frac{h_{\text{total}}}{H_0} &\approx \pm A_{ca} \sum_{j=NN} (-1)^j \chi_{AF}(\mathbf{r}_{Fe,j}) \\ &+ A_{cc} \sum_{j=NN} \chi_{RKKY}(\mathbf{r}_{Fe,j}) \end{aligned} \quad (4)$$

where  $A_{ca}$  is the off-diagonal hyperfine field form factor (Supplementary Section I) approximated to be  $A_{ca} \approx 0.027 \text{ T}/\mu_B$  [11], the plus and minus signs in front of  $A_{ca}$  correspond to Na nuclei above and below the Fe plane [10]. The susceptibility  $\chi_{RKKY}$  is given by the RKKY simulation based on Eq. 1 for the room-temperature spectrum. We fit the main component of the  $^{23}\text{Na}$  NMR spectrum of  $x = 0.012$  at  $T = 9$  K to the histogram of  $h_{\text{total}}$  given by Eq. 4 with results in Fig. 4 (a). From the fit we obtained  $C_0 \approx 1.3$ ,  $C_1 \approx 0.64$ , and  $\xi \approx 6.5d$ , indicating that the Cu dopant in NaFeAs gives rise to a magnetic perturbation that has similar magnitude but a longer range than Ni does in the Ba122 system [33], possibly due to the fact that the Cu atoms are associated with a stronger magnetic scattering potential than impurities in Ba122 [41, 42]. A lorentzian model gives similar results, also shown in Fig. 4 (a). The Cu-induced magnetic perturbation, increases with  $x$  in the doping range  $0 < x < 0.02$ , consistent with the suppression of the AFM order shown in the phase diagram (Fig. 1).

## DISCUSSION

The RKKY interaction is particularly sensitive to the electronic structure of the system. In the paramagnetic state, the frequency shift associated with each satellite appears to be following approximately the same temperature dependence down to  $\sim 125$  K (Supplementary Section IV), suggesting that the RKKY interaction is largely temperature-independent at high temperatures. However, the amplitude of the RKKY oscillation could weaken due to a spin-density-wave (SDW) gap in the AFM state [6, 19], leading to smaller hyperfine fields at the Na sites and therefore smaller frequency shifts of the satellites with respect to the main peak. This change in relative frequency shift, combined with the line broadening of the NMR spectrum, could lead to the satellite resonances being absorbed into the main peak, and therefore rendering the satellites absent in the AFM state, as shown in the experimental spectrum at  $T = 9$  K. This is in contrast to the simulated spectra for which the effect of SDW gap was not considered [Fig. 4 (a)]. A scanning tunneling microscopic study of the SDW gap in the parent compound is discussed in Ref. [43].

From the simulation results we approximated the ordered moment of the AFM background to be  $m \approx 0.003$

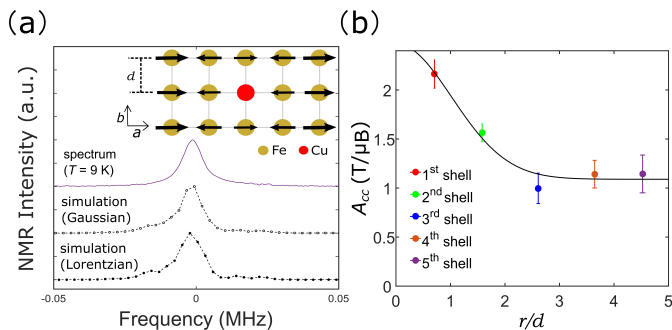


FIG. 4. Analysis of  $^{23}\text{Na}$  NMR line shapes from impurity induced perturbation of the AFM background. (a) Comparison between the  $^{23}\text{Na}$  spectrum for  $T = 9$  K and  $H_0 = 14$  T  $\parallel c$ -axis, and the simulated spectra. Both gaussian and lorentzian models were considered leading to similar length scales  $\xi \approx 6.5d$ , where  $d$  is the Fe lattice spacing. A schematic of the magnetic perturbation is shown in the inset; black arrows represent perturbed magnetic moments. (b) Dependence of the hyperfine field form factor,  $A_{cc}$ , on  $r/d$ . The solid curve represents a fit to our model for  $A_{cc}(r/d)$ .

$\mu_B/\text{Fe}$ , smaller than that approximated from the linear interpolation of the neutron scattering results for  $x = 0.016$  and the parent compound,  $m \approx 0.02 \mu_B/\text{Fe}$  [12]. This discrepancy could be partly attributed to the relatively large uncertainty associated with the moment for the parent compound. Also, the evolution of the ordered moment with doping may not be linear, as reflected for the Co-doped Na-111 system [44]. More importantly, thermal fluctuations could suppress the ordered moment probed by NMR which has a time scale at least three orders of magnitude longer than that of the neutron scattering. A NMR study extending into the superconducting state can reveal further information about the evolution of the AFM order moment at lower temperatures  $T \leq T_c$ . However, this is beyond the scope of the present article. Despite the discrepancy between the NMR and neutron scattering results, the magnetic moments given by the two measurements are both small; orders of magnitude weaker than that for a  $\text{NaFe}_{0.56}\text{Cu}_{0.44}\text{As}$  single crystal ( $m \approx 1 \mu_B/\text{Fe}$  at  $T \approx 4$  K) [12]. Such small magnetic moments in  $x \approx 0.01$  are aligned with itinerant antiferromagnetism, consistent with our analysis of the spin-lattice relaxation data. Another possible cause for the small ordered moment could be the presence of magnetic frustration [24]; however, we found no evidence for significant frustration from inhomogeneous relaxation, from our simulation, or from  $\chi(T)$ .

The conduction electrons are mainly responsible for the long-range magnetic order; however, the existence of localized moments is intrinsic to the RKKY model since the local moments are coupled through that interaction. Using the RKKY simulation results and  $K(\chi)$ , we calculate the  $r$ -dependence of the hyperfine field form factor,  $A_{cc}$  vs  $r/d$ , in Fig. 4 (b), with  $r$  being the distance from

a Cu dopant in the  $ab$ -plane. Since  $A_{cc}$  characterizes the strength of the transferred hyperfine interaction between the Fe  $3d$  electrons and the Na nuclei, its  $r$ -dependence may originate from a change in the local electron density around a Cu dopant [42, 45]. Indeed, for iron pnictides, it was demonstrated that the extra  $d$  electrons contributed by the dopants are largely localized in their near vicinity, leading to a strong increase in the electron density close to the dopant [42]. Fitting the data to the phenomenological model,  $a \exp[-(r/d)^2/(2\lambda^2)] + b$  [Fig. 4 (b)], we obtain  $\lambda \approx d$ , significantly smaller than the correlation length of the Cu-induced perturbation to the AFM order;  $\xi \approx 6.5d$ . The result of this comparison can be attributed to possible enhancement of the magnetic perturbation by the background long-range AFM order, which has a correlation length  $\xi_{\text{AF}} \gtrsim 35d$  [46]. On the other hand, in a metallic crystal, an excessive impurity potential responsible for a perturbation to the local electron density can be almost completely screened by conduction electrons within the impurity Wigner-Seitz cell [47]. Thus, the relative small value of  $\lambda$  might also be ascribed to the screening effect of the conduction electrons.

Our direct evidence for the RKKY interaction, combined with analysis of the spin-lattice relaxation rate and the Cu-induced magnetic perturbation, indicate that the picture of coexisting itinerant and localized electrons is important for understanding the magnetism in lightly Cu-doped  $\text{NaFe}_{1-x}\text{Cu}_x\text{As}$ . This is consistent with theoretical studies in pnictides showing that part of the Fe  $3d$  electrons are itinerant and the rest are localized [48–50]. Moreover, neutron scattering results show that the Bragg peak remains at a commensurate position in compounds approaching optimal doping ( $x \approx 0.02$ ) [38], which is not compatible with a purely itinerant picture where Fermi surface nesting gives rise to incommensurate magnetic order. Finally, the existence of RKKY interaction reveals commonality between metallic pnictides and other strongly correlated electron systems including heavy fermion compounds, prompting future identification of quantum criticality and study of its nature in Cu-doped  $\text{NaFe}_{1-x}\text{Cu}_x\text{As}$ .

## METHODS

The single crystals of  $\text{NaFe}_{1-x}\text{Cu}_x\text{As}$  which we performed NMR measurements on were grown by the self-flux method at Rice University [12]. Detailed information on sample preparation, including specially designed hermetic sample holders for NMR measurements, can be found elsewhere [15]. We performed  $^{23}\text{Na}$  NMR experiments for compounds  $x = 0.010$  and  $0.012$ , with an external magnetic field,  $H_0 = 13.98$  T, along the sample  $c$ -axis, the  $[001]$  direction. Since  $^{23}\text{Na}$  has a nuclear spin of  $3/2$ , we used the quadrupolar echo pulse sequence ( $\pi/2$ - $\tau$ - $\pi/2$ - $\tau$ -echo) to maximize the excitation bandwidth for

collecting NMR spectrum. The linewidth is taken to be the full width at half maximum (FWHM) of a spectrum. For  $T_2$  measurements, we varied the delay time,  $\tau$ , from 0.2  $\mu\text{s}$  to 2 ms to measure recovery profile from which  $T_2$  was extracted by fitting. A saturation-recovery sequence was used for  $T_1$  measurements. The length of  $\pi/2$  pulse length was typically set to  $\sim 6 \mu\text{s}$ .

## DATA AVAILABILITY

The data that support the findings of this study are available from the corresponding author upon reasonable request.

## ACKNOWLEDGMENT

We thank Weiyi Wang and Chongde Cao for their contributions to the crystal growth and characterization. The NMR spectrometer, MagRes2000 wide-band spectrometer system, was designed by A. P. Reyes at the National High Magnetic Field Laboratory (NHMFL). The home-built continuous flow cryostat was designed by J.A. Lee at Northwestern University. Research was supported by the U.S. Department of Energy (DOE), Office of Basic Energy Sciences (BES), Division of Material Sciences and Engineering under Award No. DE-FG02-05ER46248 (WPH) and DE-FG02-05ER46202 (PD), and the NHMFL by NSF and the State of Florida. The single crystal growth efforts at Rice were supported by the U.S. DOE, BES under Grant No. DE-SC0012311. Part of the materials work at Rice was supported by the Robert A. Welch Foundation under Grant No. C-1839.

---

\* Corresponding author. Email: yizhouxin2018@u.northwestern.edu

† Present address: Center for Correlated Matter and Department of Physics, Zhejiang University, Hangzhou, China

- [1] J. B. Boyce and C. P. Slichter, *Phys. Rev. Lett.* **32**, 61 (1974).
- [2] S. Paschen and Q. Si, *Nature Reviews Physics* **3**, 9 (2021).
- [3] C. M. Varma, *Rev. Mod. Phys.* **48**, 219 (1976).
- [4] P. Gegenwart, Q. Si, and F. Steglich, *Nature Phys* **4**, 186 (2008).
- [5] M. Hirayama, T. Misawa, T. Miyake, and M. Imada, *Journal of the Physical Society of Japan* **84**, 093703 (2015), <https://doi.org/10.7566/JPSJ.84.093703>.
- [6] A. Akbari, I. Eremin, and P. Thalmeier, *Phys. Rev. B* **84**, 134513 (2011).
- [7] S. Zapf, D. Wu, L. Bogani, H. S. Jeevan, P. Gegenwart, and M. Dressel, *Phys. Rev. B* **84**, 140503 (2011).
- [8] M. Moroni, P. Carretta, G. Allodi, R. De Renzi, M. N. Gastiasoro, B. M. Andersen, P. Materne, H.-H. Klauss, Y. Kobayashi, M. Sato, and S. Sanna, *Phys. Rev. B* **95**, 180501 (2017).
- [9] D. LeBoeuf, Y. Texier, M. Boselli, A. Forget, D. Colson, and J. Bobroff, *Phys. Rev. B* **89**, 035114 (2014).
- [10] A. F. Wang, J. J. Lin, P. Cheng, G. J. Ye, F. Chen, J. Q. Ma, X. F. Lu, B. Lei, X. G. Luo, and X. H. Chen, *Phys. Rev. B* **88**, 094516 (2013).
- [11] L. Ma, G. F. Chen, D.-X. Yao, J. Zhang, S. Zhang, T.-L. Xia, and W. Yu, *Phys. Rev. B* **83**, 132501 (2011).
- [12] Y. Song, Z. Yamani, C. Cao, Y. Li, C. Zhang, J. S. Chen, Q. Huang, H. Wu, J. Tao, Y. Zhu, *et al.*, *Nature communications* **7**, 13879 (2016).
- [13] C. E. Matt, N. Xu, B. Lv, J. Ma, F. Bisti, J. Park, T. Shang, C. Cao, Y. Song, A. H. Nevidomskyy, P. Dai, L. Patthey, N. C. Plumb, M. Radovic, J. Mesot, and M. Shi, *Phys. Rev. Lett.* **117**, 097001 (2016).
- [14] S. Zhang, Y. He, J.-W. Mei, F. Liu, and Z. Liu, *Phys. Rev. B* **96**, 245128 (2017).
- [15] Y. Xin, I. Stolt, J. A. Lee, Y. Song, P. Dai, and W. P. Halperin, *Phys. Rev. B* **99**, 155114 (2019).
- [16] Y. Xin, I. Stolt, Y. Song, P. Dai, and W. P. Halperin, *Phys. Rev. B* **101**, 064410 (2020).
- [17] Y. Song, W. Wang, E. Paris, X. Lu, J. Pelliciani, Y. Tseng, Y. Huang, D. McNally, M. Dantz, C. Cao, R. Yu, R. J. Birgeneau, T. Schmitt, and P. Dai, *Phys. Rev. B* **103**, 075112 (2021).
- [18] S. T. Cui, S. Kong, S. L. Ju, P. Wu, A. F. Wang, X. G. Luo, X. H. Chen, G. B. Zhang, and Z. Sun, *Phys. Rev. B* **88**, 245112 (2013).
- [19] M. Yi, D. H. Lu, R. G. Moore, K. Kihou, C.-H. Lee, A. Iyo, H. Eisaki, T. Yoshida, A. Fujimori, and Z.-X. Shen, *New Journal of Physics* **14**, 073019 (2012).
- [20] Y.-Z. Zhang, I. Opahle, H. O. Jeschke, and R. Valentí, *Phys. Rev. B* **81**, 094505 (2010).
- [21] I. I. Mazin, D. J. Singh, M. D. Johannes, and M. H. Du, *Phys. Rev. Lett.* **101**, 057003 (2008).
- [22] F. L. Ning, K. Ahilan, T. Imai, A. S. Sefat, M. A. McGuire, B. C. Sales, D. Mandrus, P. Cheng, B. Shen, and H.-H. Wen, *Phys. Rev. Lett.* **104**, 037001 (2010).
- [23] D. C. Johnston, *Advances in Physics* **59**, 803 (2010), <https://doi.org/10.1080/00018732.2010.513480>.
- [24] Q. Si and E. Abrahams, *Phys. Rev. Lett.* **101**, 076401 (2008).
- [25] T. Yildirim, *Phys. Rev. Lett.* **101**, 057010 (2008).
- [26] S.-P. Kou, T. Li, and Z.-Y. Weng, *EPL (Europhysics Letters)* **88**, 17010 (2009).
- [27] S. Li, C. de la Cruz, Q. Huang, G. F. Chen, T.-L. Xia, J. L. Luo, N. L. Wang, and P. Dai, *Phys. Rev. B* **80**, 020504 (2009).
- [28] A. Akbari, P. Thalmeier, and I. Eremin, *New Journal of Physics* **15**, 033034 (2013).
- [29] Y. Song, Z. Yamani, C. Cao, Y. Li, C. Zhang, J. Chen, Q. Huang, H. Wu, J. Tao, Y. Zhu, *et al.*, arXiv preprint arXiv:1504.05116 **7** (2015).
- [30] M. A. Ruderman and C. Kittel, *Phys. Rev.* **96**, 99 (1954).
- [31] J. B. Boyce and C. P. Slichter, *Phys. Rev. B* **13**, 379 (1976).
- [32] A. Jagannathan, E. Abrahams, and M. J. Stephen, *Phys. Rev. B* **37**, 436 (1988).
- [33] A. P. Dioguardi, N. apRoberts Warren, A. C. Shockley, S. L. Bud'ko, N. Ni, P. C. Canfield, and N. J. Curro, *Phys. Rev. B* **82**, 140411 (2010).

- [34] A. P. Dioguardi, J. Crocker, A. C. Shockley, C. H. Lin, K. R. Shirer, D. M. Nisson, M. M. Lawson, N. Roberts-Warren, P. C. Canfield, S. L. Bud'ko, S. Ran, and N. J. Curro, *Phys. Rev. Lett.* **111**, 207201 (2013).
- [35] S. Oh, A. M. Mounce, W. P. Halperin, C. L. Zhang, P. Dai, A. P. Reyes, and P. L. Kuhns, *Phys. Rev. B* **85**, 174508 (2012).
- [36] S. Oh, A. M. Mounce, J. A. Lee, W. P. Halperin, C. L. Zhang, S. Carr, and P. Dai, *Phys. Rev. B* **87**, 174517 (2013).
- [37] T. Moriya and K. Ueda, *Solid State Communications* **15**, 169 (1974).
- [38] G. Tan, Y. Song, R. Zhang, L. Lin, Z. Xu, L. Tian, S. Chi, M. K. Graves-Brook, S. Li, and P. Dai, *Phys. Rev. B* **95**, 054501 (2017).
- [39] A. Charnukha, Z. P. Yin, Y. Song, C. D. Cao, P. Dai, K. Haule, G. Kotliar, and D. N. Basov, *Phys. Rev. B* **96**, 195121 (2017).
- [40] N. J. Curro, P. C. Hammel, B. J. Suh, M. Hücker, B. Büchner, U. Ammerahl, and A. Revcolevschi, *Phys. Rev. Lett.* **85**, 642 (2000).
- [41] A. F. Kemper, C. Cao, P. J. Hirschfeld, and H.-P. Cheng, *Phys. Rev. B* **80**, 104511 (2009).
- [42] H. Wadati, I. Elfimov, and G. A. Sawatzky, *Phys. Rev. Lett.* **105**, 157004 (2010).
- [43] X. Zhou, P. Cai, A. Wang, W. Ruan, C. Ye, X. Chen, Y. You, Z.-Y. Weng, and Y. Wang, *Phys. Rev. Lett.* **109**, 037002 (2012).
- [44] G. Tan, Y. Song, C. Zhang, L. Lin, Z. Xu, T. Hou, W. Tian, H. Cao, S. Li, S. Feng, and P. Dai, *Phys. Rev. B* **94**, 014509 (2016).
- [45] S. Ideta, T. Yoshida, I. Nishi, A. Fujimori, Y. Kotani, K. Ono, Y. Nakashima, S. Yamaichi, T. Sasagawa, M. Nakajima, K. Kihou, Y. Tomioka, C. H. Lee, A. Iyo, H. Eisaki, T. Ito, S. Uchida, and R. Arita, *Phys. Rev. Lett.* **110**, 107007 (2013).
- [46] W. Wang, Y. Song, C. Cao, K.-F. Tseng, T. Keller, Y. Li, L. W. Harriger, W. Tian, S. Chi, R. Yu, *et al.*, *Nature communications* **9**, 1 (2018).
- [47] J. Galsin, *Solid State Physics: An Introduction to Theory* (Elsevier Science, 2019).
- [48] W.-G. Yin, C.-C. Lee, and W. Ku, *Phys. Rev. Lett.* **105**, 107004 (2010).
- [49] J. Wu, P. Phillips, and A. H. Castro Neto, *Phys. Rev. Lett.* **101**, 126401 (2008).
- [50] L. de'Medici, S. R. Hassan, and M. Capone, *Journal of superconductivity and novel magnetism* **22**, 535 (2009).

### AUTHOR CONTRIBUTIONS

The NMR experiments and analysis work were carried out by Y.X. with assistance from I.S., under the supervision of W.P.H. Most of the single-crystal growth was carried out by Y.S., under the supervision of P.D. The paper was written by Y.X. and W.P.H. All authors assisted in manuscript preparation.

### ADDITIONAL INFORMATION

#### Competing financial interests:

The authors declare no competing financial interests.